Materials Science and Engineering C 58 (2016) 1246–1254

Contents lists available at ScienceDirect

Materials Science and Engineering C

journal homepage: www.elsevier.com/locate/msec

Nano-assemblies consisting of Pd/Pt nanodendrites and poly (diallyldimethylammonium chloride)-coated reduced graphene oxide on glassy carbon electrode for hydrogen peroxide sensors

Yanyan Zhang, Cong Zhang, Di Zhang, Min Ma, Weizhen Wang, Qiang Chen *

The Key Laboratory of Bioactive Materials, Ministry of Education, College of Life Science, Nankai University, Weijin Road No. 94, Tianjin 300071, China

ARTICLE INFO

Article history:
Received 15 June 2015
Received in revised form 12 August 2015
Accepted 2 September 2015
Available online 7 September 2015

Keywords:
Hydrogen peroxide biosensor
Graphene
Palladium nanocrystal
Platinum nanodendrite

ABSTRACT

Non-enzymatic hydrogen peroxide (H_2O_2) sensors were fabricated on the basis of glassy carbon (GC) electrode modified with palladium (Pd) core-platinum (Pt) nanodendrites (Pt-NDs) and poly (diallyldimethylammonium chloride) (PDDA)-coated reduced graphene oxide (rGO). A facile wet-chemical method was developed for preparing Pd core-Pt nanodendrites. In this approach, the growth of Pt NDs was directed by Pd nanocrystal which could be regarded as seed. The PDDA-coated rGO could form uniform film on the surface of GC electrode, which provided a support for Pd core- Pt NDs adsorption by self-assembly. The morphologies of the nanocomposites were characterized by transmission electron microscopy, energy-dispersive X-ray spectroscopy and X-ray diffraction (spectrum). Electrocatalytic ability of the nanocomposites was evaluated by cyclic voltammetry and chronoamperometric methods. The sensor fabricated by Pd core-Pt NDs/PDDA-rGO/GCE exhibited high sensitivity (672.753 μA mM^{-1} cm^{-2}), low detection limit (0.027 μM), wider linear range (0.005–0.5 mM) and rapid response time (within 5 s). Besides, it also exhibited superior reproducibility, excellent anti-interference performance and long-term stability. The present work could afford a viable method and efficient platform for fabricating all kinds of amperometric sensors and biosensors.

1. Introduction

The detection of hydrogen peroxide (H_2O_2) makes a great difference in many aspects including food safety control, medical and pharmaceutical fields [1,2] and cosmetic areas. Therefore, for the determination of H_2O_2, a lot of analytical techniques have been raised, such as spectrophotometry [3], typical chemiluminescence [4], common titrimetry [5] and electrochemical approaches [6–9]. Among these analytical techniques, electrochemical approaches have been widely used for determination of H_2O_2 owing to its unique simplicity, superior sensitivity, and excellent selectivity. During the past few decades, electrochemical biosensors on the basis of enzyme have been extensively applied in H_2O_2 determination [10]. However, many disadvantages were found, such as limited stability, low reproducibility and high cost. On the other hand, non-enzymatic H_2O_2 sensors based on nanocomposites have attracted much attention due to its rapid response, long-term stability and low cost. Therefore, the development of catalytic materials with excellent catalyst activity is still a challenge in the development of non-enzymatic H_2O_2 sensors.

Recently, hybrid nanocomposites have appealed to wide interest owing to their distinct electrochemical, magnetic and physical properties that substantially differ from those of corresponding monometallic components [11–13]. Tailored functionalities could be developed to satisfy a particular application by rationally designing such hybrid nanomaterials [14,15]. Pt nanomaterials with large surface area exhibit excellent conductivity and electrocatalytic activities [16]. Besides, Pt is one of the most effective catalysts to facilitate H_2O_2 reduction [17]. Consequently, there has been growing interests in using Pt nanomaterials to prepare H_2O_2 sensors. The size and shape of nanocrystals are most important parameters to contribute to the catalytic property [18]. All kinds of chemical protocols have been developed for preparing nanocrystals in cube [19], tube [20], wire [21], mesoporous [22] and dendrite [23]. Among Pt nanomaterials, nanodendrites attract particular interests owing to their excellent catalytic activity. On the other hand, in order to further take full advantage of the catalytic property of Pt and decrease the use of previous Pt as soon as possible, it is very necessary to combine Pt nanodendrites with other efficient electron transfer materials such as Pd [24].

Graphene are of particular promise in biosensor and electrochemical application owing to it possesses single-atom thickness and better electron conductivity [25,26]. In previous reports, graphene-modified electrodes displayed excellent electrocatalytic activity for H_2O_2, glucose, nitrite and other important electroactive species [27–29]. In order to

* Corresponding author.
E-mail address: qiangchen@nankai.edu.cn (Q. Chen).

http://dx.doi.org/10.1016/j.msec.2015.09.015
0928-4931/

prepare graphene sheets, various methods have been developed, such as chemical vapor deposition [30], the mechanical incision of bulk graphite [31], epitaxial growth [32] and intercalation by using of polymers, solvents [33] or surfactants [34]. Up to now, the most popular method to produce graphene sheets for quantity application may be a wet chemical reduction of graphene oxide [15]. In this paper, we use hydrazine to reduce graphene oxide to provide reduced graphene oxide. The decoration of graphene with bimetallic nanocomposites can offer a great opportunity to increase electrocatalytic ability and accelerate electron transfer rate between detection molecules and electrode.

As we all know, nanomaterials are easy to aggregate and produce bulk, which result in decrease electrocatalytic ability obviously. Therefore, it is necessary for choosing suitable dispersant to scatter prepared nanomaterials. Poly (diallyldimethylammonium chloride) (PDDA) is a water-soluble, biocompatible, readily available low-cost cationic polymer with good chemical property and thermal stability. PDDA as a dispersant combined with nanomaterial by electrostatic interaction for forming homogeneous dispersion achieving the effect of accelerating electron transfer rate.

Here, we synthesized Pt/Pd nanodendrites (NDs) consisting of orderly array of Pt NDs on the core of Pd. In this method, Pd nanocrystals (Pd NCs) were regarded as seeds to direct the growth of Pt NDs with Pt branches grown by L-ascorbic acid reduction of K_2PtCl_4 in aqueous solution. However, nanocrystals easily form aggregation, leading to decrease in catalytic activity. We chose PDDA as dispersant for producing homogeneous suspension. As far as we know, there were few papers reporting the catalytic property of Pd core-Pt NDs and PDDA-rGO for H_2O_2 sensor fabrication. This paper reports that H_2O_2 sensors based on Pd core-Pt NDs and PDDA-rGO exhibit much higher response.

2. Experimental

2.1. Reagents

Na_2PdCl_4 and Poly (diallydimethylammonium chloride) were purchased from Aldrich Co. (USA). Graphene oxide (GO) was purchased from Nanjing XFNANO Materials Tech Co., Ltd. (China). Aqueous solution of hydrogen peroxide was purchased from Tianjin Chemical Reagent Co. L-ascorbic acid and $K_2PtCl_4 \cdot 3H_2O$ were bought from Sigma Co. (USA). Na_2HPO_4 and NaH_2PO_4 were used to prepare phosphate buffer solution (PBS, 0.1 M, pH 7.0). All aqueous solutions were prepared by doubly distilled water. All other reagents used without further purification and were of analytical grade. All experiments in this report were performed at room temperature.

2.2. Measurements

A typical one-compartment cell equipped with a 283 Potentiostat–Galvanostat electrochemical workstation (EG & GPARC with M 270 software) was employed to all electrochemical experiments at room temperature. Pd core-Pt NDs-PDDA-rGO-modified GC electrode (3 mm diameter) was used for working electrode, a Pt wire (1 mm diameter) was used for auxiliary electrode, and Ag/AgCl (saturated with KCl) was used for reference electrode, which form a conventional three-electrode system. And the conventional three-electrode system was drawn upon all electrochemical experiment. A Rigaku D/max-rA with Cu Kα radiation on a diffractometer (Rigaku, Japan) was used to record X-ray diffraction (XRD) patterns. Besides, transmission electron microscopy (TEM) images were gathered on Tecnai G2 F20 instrument (Philips, Holland), which is equipped with an energy-dispersive X-ray spectroscopy (EDX) analyzer and scan electron microscopy (SEM, QUANTA 200, FEI Co.) was used for recording the surface morphology.

2.3. Preparation of PDDA-functionalized rGO

40 mg of GO was dissolved in 40 mL of PDDA solution (0.2%) by ultrasonication for 90 min, then stirred for 12 h to obtain homogeneous PDDA-GO aqueous dispersion (1 mg/mL). 400 μL of hydrazine solution (32 mM) was mixed with the PDDA-GO dispersion. The mixture was heated at 100 °C for 36 h. Finally, the resulting black dispersion was centrifuged at 15,000 rpm for 45 min and the precipitated material was successively rinsed with ethanol and doubly distilled water with the help of centrifugation at 10,000 rpm for 30 min. PDDA-rGO thus obtained was suspended in doubly distilled water at 1 mg/mL.

2.4. Preparation of Pd core-Pt NDs

The Pd core-Pt NDs were prepared from a seed-mediated approach described previously [35]. Briefly, 57 mg of K_2PdCl_4 was dissolved in doubly distilled water, followed by adding 8 mL of solution consisting of 60 mg of L-ascorbic acid, 105 mg of PVP, and 60 mg of citric acid. The resulting mixture was heating at 100 °C for 3 h to obtain Pd NCs with an average size of 5 nm. Then, 4 mL of Pd NCs was mixed with 24 mL of aqueous solution containing 140 mg of PVP and 240 mg of L-ascorbic acid, followed by treatment at 90 °C. Finally, 108 mg of K_2PtCl_4 solution was rapidly injected into resulting mixture under stirring, and heated for 3 h to produce Pd core-Pt NDs. The final products were washed with doubly distilled water followed centrifugation at 20,000 rpm for 30 min. In order to forming homogeneous Pd core-Pt nanodendrites, PDDA was hybridized with Pd core-Pt nanodendrites (1:1) by ultrasonication for 3 h. By centrifugation at 20,000 rpm for 30 min, PDDA-Pd core-Pt nanodendrites were obtained, and the resulted were suspended in doubly distilled water at 1 mg/mL. According to above process, in the absence of Pd NCs, Pt nanoparticles (Pt NPs) at 1 mg/mL were synthesized.

2.5. Fabrication of H_2O_2 sensor

GC disk electrode (3 mm diameter) employed in this report was polished by powder of aluminum oxide, and ultrasonically rinsed with absolute ethanol. The polished electrode was dried with nitrogen gas. The surface of polished GC electrode was modified with 5 μL of PDDA-rGO dispersion, then, dried to obtain PDDA-rGO-modified GC electrode. Then, 5 μL of Pd core-Pt dendrite dispersion was dropped onto the surface of PDDA- rGO-modified GC electrode to obtain Pd core-Pt NDs/PDDA-rGO-modified electrodes. In Scheme 1, the approach of fabrication is illustrated. As comparison, the surface of polished GC electrode was modified with 5 μL of Pt NPs (1 mg/mL), then dried to obtain Pt NPs-modified GC electrode.

3. Results and discussion

3.1. Morphologies of the synthesized PDDA-rGO and Pd core-Pt NDs

The morphologies of the PDDA-rGO sheets were characterized by TEM and SEM, Pd NCs and Pd core-Pt NDs were characterized by TEM at different magnifications. Fig. 1A and B show that PDDA-rGO was presented as transparent thin films signifying it was entirely exfoliated in the aqueous solution. Fig. 1C and D demonstrate that the average diameter of small Pd NPs was 5 nm. In Fig. 1E, the high-resolution TEM (HRTEM) image of Pd NPs shows that the lattice fringes of every Pd NP are paralleled and have the same orientation, and further indicates they were single crystal. Typical TEM images (Fig. 1F and G) of Pd core-Pt NDs reveal that a lot of Pt branches have grown by directing of Pd core. In order to further figure out the microscopic detailed structure of Pt core-Pd NDs, HRTEM image of the nanocomposite was recorded (Fig. 1H), in which Pt nanodendrites clearly displayed at different sites on the core. The diameter of Pt nanodendrite (circled part) is

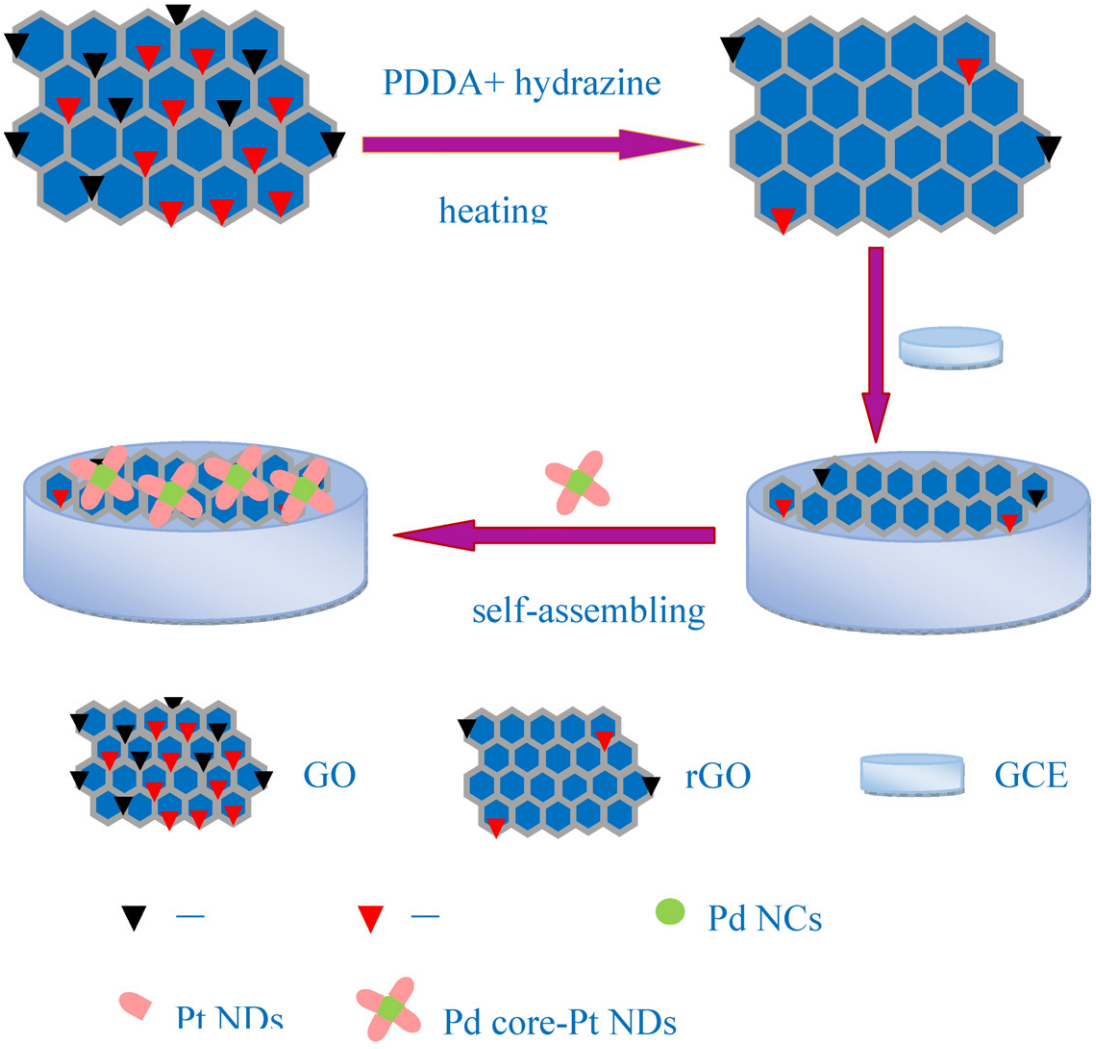

Scheme 1. A schematic illustration for the preparation of PDDA-rGO/Pd core-Pt NDs modified glassy carbon electrode.

3–6 nm and highly ordered and continuous fringe patterns of signal crystal can be seen.

Fig. 2A exhibits energy dispersive x-ray spectroscopy (EDX) result of a single Pd-Pt nanoparticle, which confirms that the bimetallic nanostructure contains the elements of Pd and Pt. O peak and Cu peak were appeared resulted from the substrate. XRD patterns of Pd NCs and Pt core-Pd NDs were shown in Fig. 2B. In the XRD pattern of Pd NCs (a), peaks locate at $2\theta = 40.118°$, 46.685° and 68.119° which are assigned to the (111), (200) and (220) lattice plane of the Pd NCs respectively. The image also demonstrates that the (111) lattice plane is primary part and, the interplanar spacing of lattice fringes by measured are 0.24 nm, which correspond to the HRTEM of Pd NC in Fig. 1D. The diffraction patterns of Pd NCs and Pt core-Pd NDs (b) have similar diffraction peaks, however, the diffraction peak intensity of Pt core-Pd NDs is lower, possibly because of that the graft of Pt nanodendrites result in radiation diffusion. The results imply the Pd NCs exist in the form of core rather than alloy, in accord with the image of EDX in Fig. 2A. On the other hand, peak of Pt nanodendrites did not appear probably due to homogeneous dispersion of Pt nanodendrites in PDDA.

The orderly array of Pt branches could be caused by an autocatalytic process in which Pt progressively reduction by the seeds directing [36] and the process has explained the formation of branched and other porous nanostructures of Pt [37]. In this approach, L-ascorbic acid was used to reduced K_2PtCl_4 in the presence of seeds (Pd NCs) to generate Pt nanoparticles on the (111), (200) and (220) faces of Pd NCs. The Pt nanoparticles grown at early stage can be regarded as Pt nuclei which could provide deposition sites for further catalyzing Pt precursor. According to theory of surface-energy minimization, while continuously heat the dispersion of Pt nanoparticles at appropriate temperatures, the minor nanoparticles progressively deposited on the Pt nuclei along developing Pt branches, as above clarified, the process was known as Ostwald ripening [38]. However, without Pd NCs, a large number of Pt precursor aggregated with each other resulting in the forming of disordered Pt NPs. The Pd seeds provided various deposition sites for Pt nanodendrites that array orderly, unlike the Pt NPs synthesized in the absence of Pd NCs.

3.2. Electrochemical activity of PDDA-rGO/Pd core-Pt NCs/GCE

Ferricyanide system measured by cyclic voltammetry (CV) is an efficient and convenient approach to evaluate the effective surface area of various modified electrodes [39]. CVs of rGO-modified GC electrode (a), Pd core-Pt NDs-modified GC electrode (b), unmodified (c), PDDA-rGO-modified GC electrode (d), PDDA-rGO/Pd core-Pt NDs-modified GC electrode (e), PDDA-modified GC electrode (f) and PDDA-Pd core-Pt NDs-modified GC electrode (g) were operated in 0.1 M KCl aqueous

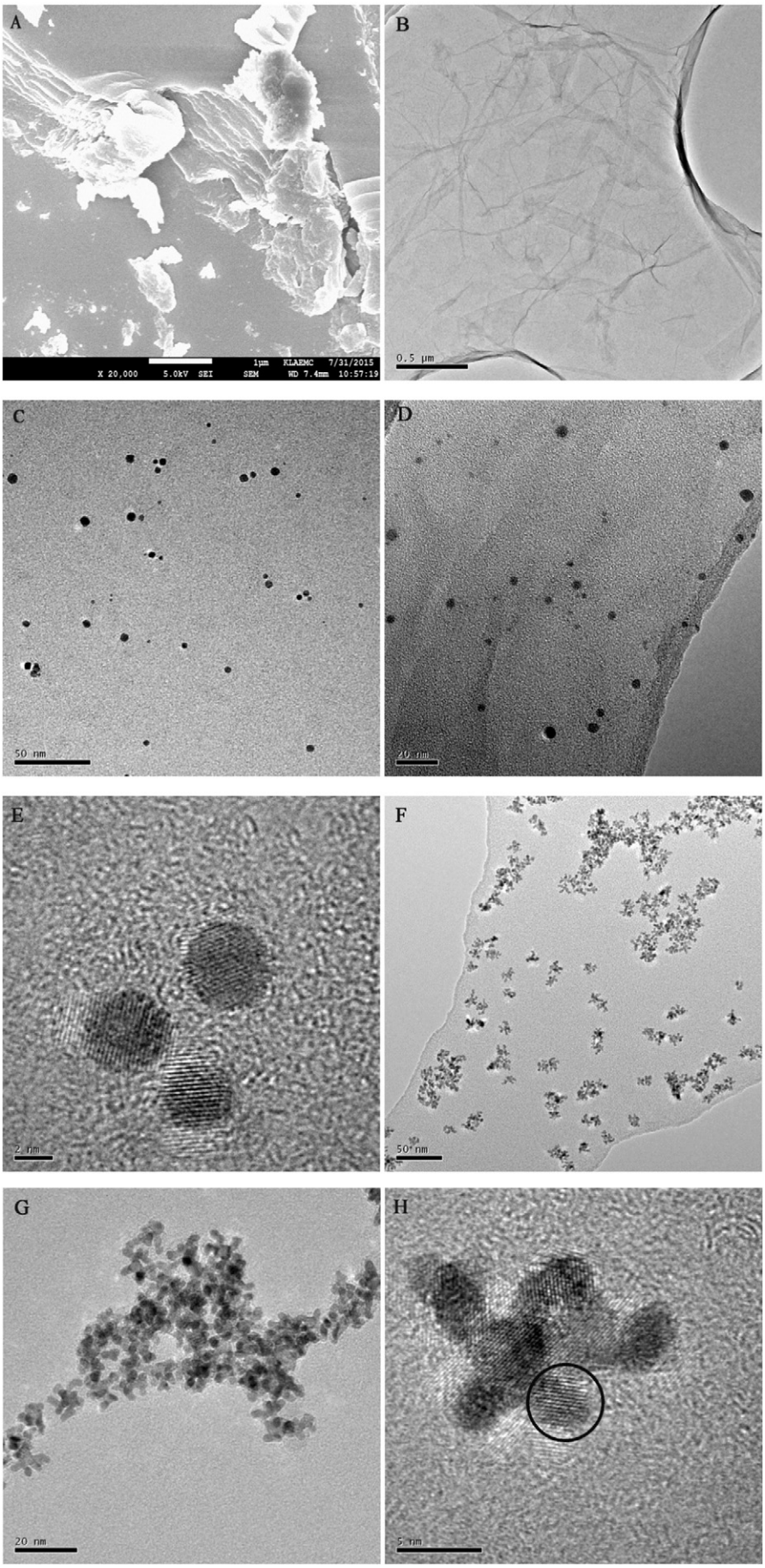

Fig. 1. SEM image of PDDA-rGO (A), TEM images of PDDA-rGO (B), Pd NCs under different magnifications (C, D and E) and Pd core-Pt NDs (F and G), HRTEM image of Pd core-Pt NDs (H).

solution containing 10 mM $[Fe(CN)_6]^{3-}$ ions (Fig. 3). For the PDDA-rGO/Pd core-Pt NDs-modified GC electrode, at 289 and 151 mV, a well-defined redox peaks were observed. As we all know, effective electroactive area is an important parameter for evaluating the property of working electrodes, herein electroactive area was calculated in accordance with Randles–Sevcik equation [40].

$$I_p = 2.69 \times 10^5 A D^{1/2} n^{3/2} \gamma^{1/2} C \quad (1)$$

where A corresponds to effective electroactive surface area of working electrode (cm^2), D represents the diffusion coefficient referring to the probe molecule in determined solution, and it approximately is 6.70×10^{-6} cm^2 s^{-1}, n is the amount of electron which transfer in the reaction, the value is equal to 1, γ is the scan rate ($V\ s^{-1}$), C is the concentration of detected molecule, in this system the concentration of detected molecule is 10 mM and I_p represents the current of redox peak. In terms of the equation explained above, we can estimate the microscopic effective electroactive surface area of PDDA-rGO/Pd core-Pt NDs-modified GC electrode to be 0.13 cm^2, which is 1.16 and 1.41 times higher than PDDA-rGO-modified and unmodified GC electrodes, respectively. Above data reveals that the PDDA-rGO/Pd core-Pt NDs nanostructures are more advantageous to accelerate electron transfer rate between the modified electrode and $[Fe(CN)_6]^{3-}$. This may be caused by the synergy effects of rGO (large surface area, superior conductivity, and unique single-atom thickness) and Pd core-Pt NDs (excellent catalytic activity and huge surface area). Satisfactory electrocatalytic activity of PDDA-rGO/Pd core-Pt NDs-modified GC electrode indicates that the nanocomposites can be used as modified electrode materials for electrochemical analysis. Besides, the microscopic effective electroactive surface area of PDDA-rGO-modified GC electrode is 3.8 times higher than rGO-modified GC electrode and PDDA-Pd core-Pt NDs-modified GC electrode is 1.5 times higher than Pd core-Pt NDs-modified GC electrode, confirming that PDDA plays an important role in developing electrochemical property. This may because that the aggregation of nanocomposites results in decrease the rate of electron transfer, PDDA as soluble cationic polymer can combine with Pd-core-Pt NDs by electrostatic interaction. Therefore, PDDA was used as dispersant for forming homogeneous dispersion, which plays an importance role in accelerating electron transfer.

3.3. Cyclic voltammetric electrochemical response of PDDA-rGO/Pd core-Pt NDs-modified GC electrode to H_2O_2

The cyclic voltammetric electrochemical response of the PDDA-rGO/Pd core-Pt NDs-modified electrode to H_2O_2 was studied under nitrogen atmosphere. Fig. 4 shows the CVs of Pt NPs- (a), Pd core-Pt NDs-modified electrodes (b) and PDDA-rGO/Pd core-Pt NDs-modified electrode (c). The Pd core-Pt NDs-modified electrode obviously increase in the reduction current around centered at 0 mV as compared with Pt NPs modified electrode. Thus, this is a clear evidence for higher activity of Pd core-Pt NDs than Pt NPs in electrolysis of H_2O_2. The potential-independent current is produced, which can be explained [41] by hypothesis of H_2O_2 reduction started by the process of dissociative adsorption as shown in Eq. (2).

$$2Pt + H_2O_2 \xrightarrow{k1} 2Pt{-}OH \quad (2)$$

$$4Pt{-}OH \xrightarrow{k2} 4Pt + O_2 + 2H_2O \quad (3)$$

The reaction (2) is followed by the reaction (3) for the reduction of H_2O_2 on Pt NDs. For the PDDA-rGO/Pd core-Pt NDs-modified electrode (c), the highest response was observed, showing that the PDDA-rGO/Pd core-Pt NDs-modified electrode exhibits the highest activity towards H_2O_2 reduction. This further verifies that the synergistic effect between PDDA-rGO and Pd core-Pt NDs, probably owing to large amounts of active sites and facilitate the contact with H_2O_2 for the electrolysis.

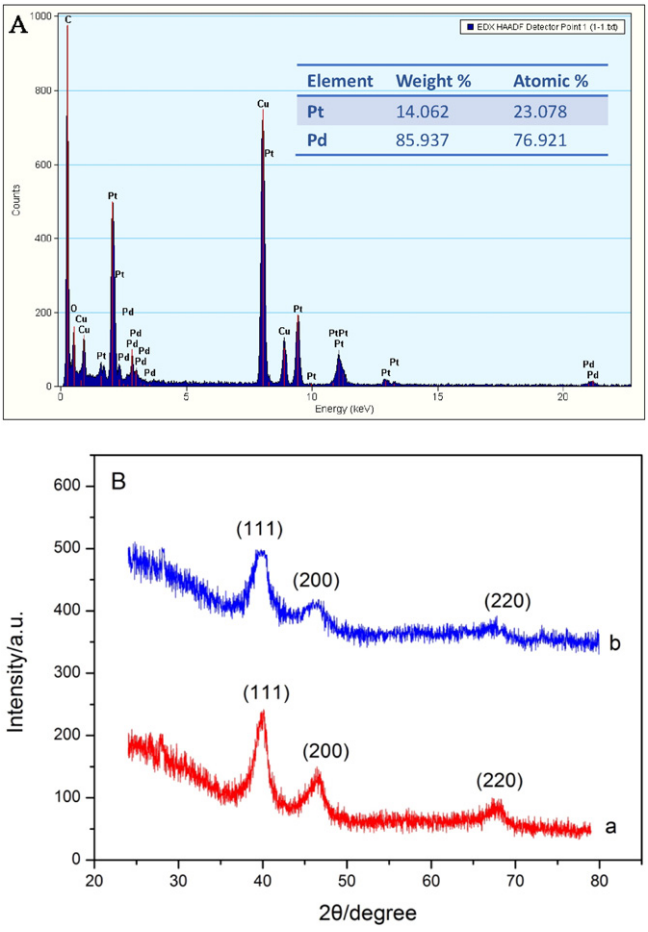

Fig. 2. EDX analysis of Pd core-Pt NDs (A) and XRD patterns (B), XRD pattern of Pd NCs (a) and XRD pattern of Pd core-Pt NDs (b).

The transfer coefficient (α) value was calculated via Eq. (4) and α found to be 0.41. Using the Eq. (5) [42], an apparent standard heterogeneous rate constant, $k_s = 48.2\ s^{-1}$, was estimated for PDDA-rGO/Pd core-Pt NDs-modified GC electrode.

$$E_p - E_{p/2} = 48/(\alpha n_a) \quad (4)$$

where E_p is the cathodic peak potential and $E_{p/2}$ is the half-peak potential.

$$\lg k_s = \alpha \lg(1-\alpha) + (1-\alpha)\lg \alpha - \lg (RT/nFv) - \alpha(1-\alpha)\ n\Delta E/2.3\ R\ T \quad (5)$$

The effect of scan rate on the electrocatalytic ability of PDDA-rGO/Pd core-Pt NDs-modified GC electrode for H_2O_2 was investigated by voltammetry (Fig. 5A). As shown in Fig. 5A, as scan rate increase, the potential of cathodic peak close to negative potentials gradually, confirming the kinetic limitation in the electrochemical reaction. Besides, a plot of peak current (I_p) vs. the square root of scan rate ($v^{1/2}$) (Fig. 5B) was shown to be linear in the range of 10–70 mV s^{-1}, suggesting that at sufficient overpotential, the process is diffusion controlled rather than surface controlled. The Tafel slope (b) was obtained from the slope of E_p vs. log v (Fig. 5C) using Eq. (6) [43]:

$$E_p = b/2 \log v + \text{constant} \quad (6)$$

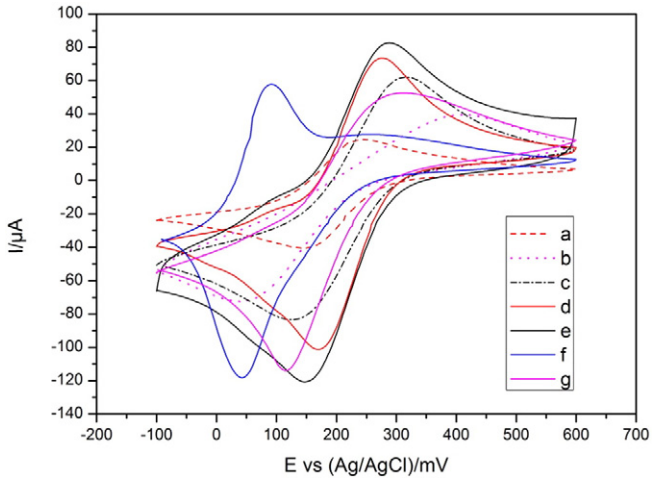

Fig. 3. CVs of rGO-modified GC electrode (a), Pd core-Pt NDs-modified GC electrode (b), unmodified (c), PDDA-rGO-modified GC electrode (d), PDDA-rGO/Pd core-Pt NDs-modified GC electrode (e), PDDA-modified GC electrode (f) and PDDA-Pd core-Pt NDs-modified GC electrode recorded (g) in 0.1 M KCl solution containing 10 mM $[Fe(CN)_6]^{3-}$. Scan rate: 50 mV s^{-1}.

The Tafel slope was calculated to be 91.8 mV, indicating that a one-electron transfer process is the rate limiting step assuming a transfer coefficient is about 0.41.

3.4. Chronoamperometric response of PDDA-rGO/Pd core-Pt NDs-modified GC electrode to H_2O_2

As we all know, the pH of the solution makes a great difference in the determination of H_2O_2. In 0.1 M PBS (N_2 saturated) with pH 4, 4.5, 5, 5.5, 6, 7, 7.5 and 8.0, the effect of pH on cathodic peak current of H_2O_2 was tested. Fig. 6 shows that cathodic peak current increase with the increase of solution PH from 4.0 to 7.0 and decrease after 7.0. For achieving optimized condition, PBS of pH 7.0 was used in subsequent experiments.

As shown in Fig. 4(c), PDDA-rGO/Pd core-Pt NDs-modified electrode exhibited the highest current at 18 mV. Therefore, the working potential was set at 18 mV for the detection of H_2O_2. Compared with other H_2O_2 amperometric sensors [11,44], the applied potential for the PDDA-rGO/Pd core-Pt NDs-modified electrodes was much lower, in which the background current could be minimized and interference from other electroactive species can be minimized. Before testing, all experimental solutions were bubbled with pure nitrogen for 10 min.

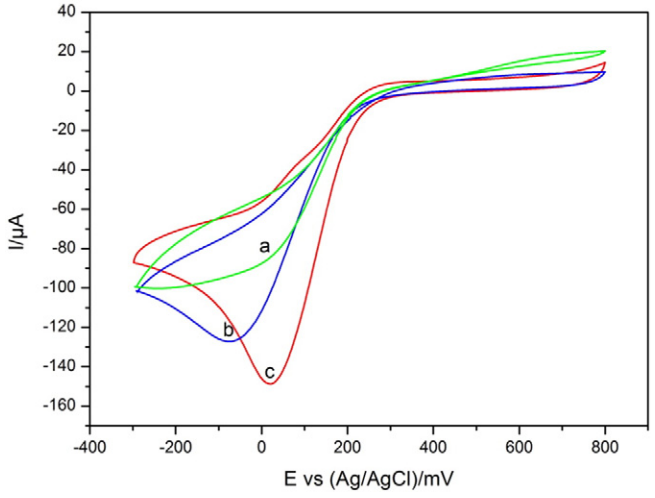

Fig. 4. CVs of Pt NPs-modified GC electrode (a), Pd core-Pt NDs-modified GC electrode (b) and PDDA-rGO/Pd core-Pt NDs-modified GC electrode (c) in PBS containing 5 mM H_2O_2.

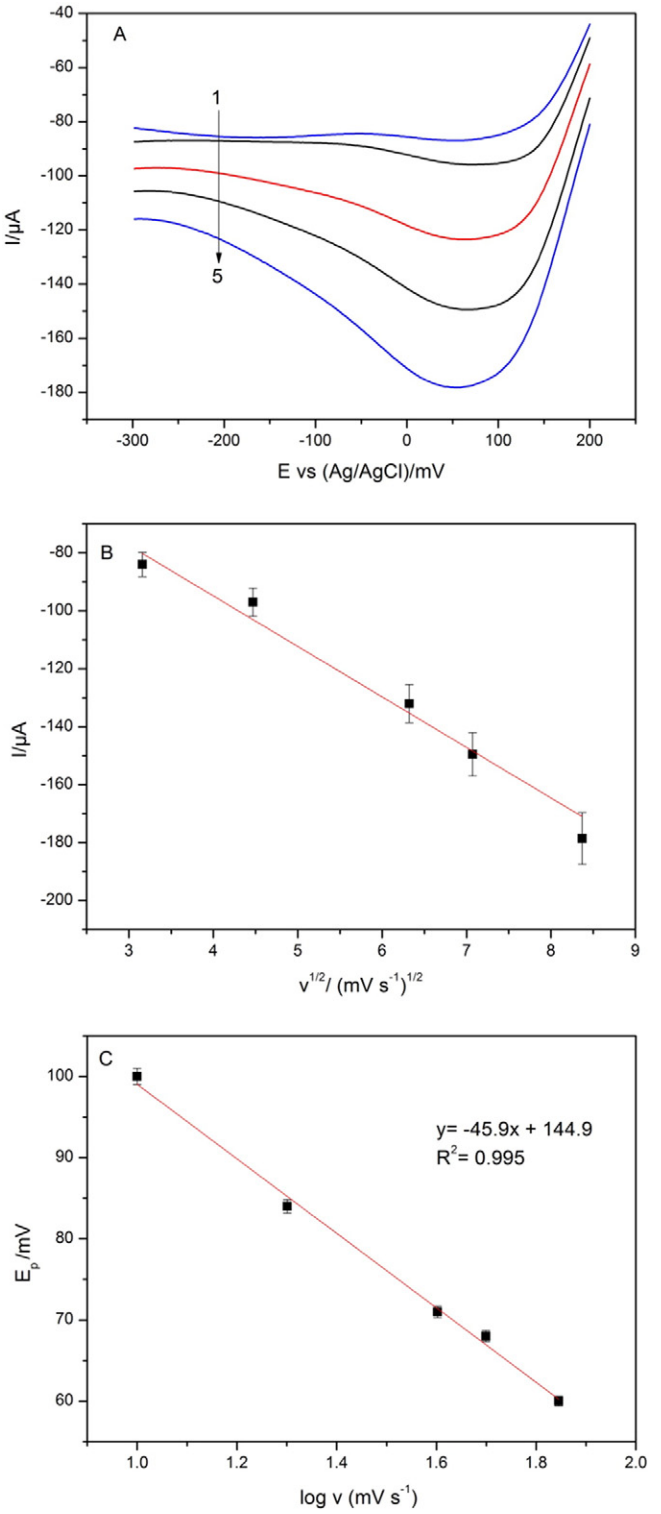

Fig. 5. CVs of PDDA-rGO/Pd core-Pt NDs-modified GC electrode in PBS containing 5 mM H_2O_2 at various scan rates from inner to outer scan rates of 10, 20, 40, 50 and 70 mV s^{-1} respectively (A), variation of cathodic peak current vs. $v^{1/2}$ (B) and cathodic peak potential vs. log v (C).

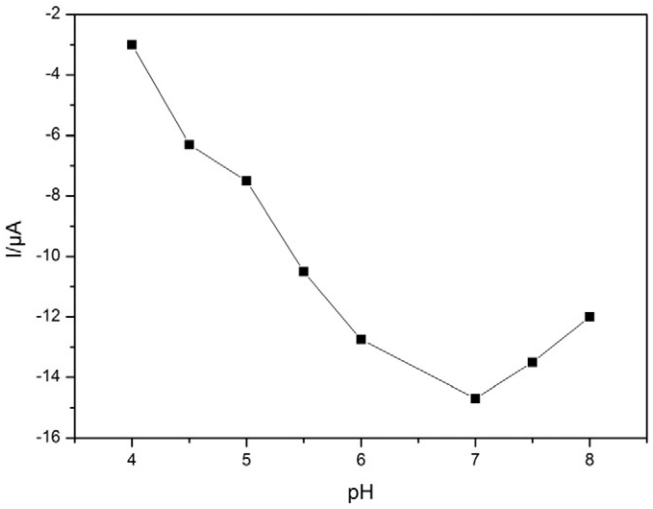

Fig. 6. The influence of pH on the cathodic peak current for H_2O_2 in PBS (scan rate: 50 mV s^{-1}).

Fig. 7A displays amperometric response of PDDA-rGO/Pd core-Pt NDs-modified GC electrode as successive addition of H_2O_2. For comparison, amperometric response of PDDA-rGO/Pt NDs-modified GC electrode and PDDA-rGO/Pd NPs-modified GC electrode were showed in Fig. 7B and C. When H_2O_2 were added every time, the PDDA-rGO/Pd core-Pt NDs-modified electrode reached a steady-stage current within 5 s, which indicated a rapid response of PDDA-rGO/Pd core-Pt NDs-modified electrode. The H_2O_2 concentration was proportional to current response in the range from 0.005 mM to 0.5 mM. In the proportion relation, the slope is 47.53 μA mM^{-1} and the correlation coefficient is 0.993. The sensitivity reached to 672.753 μA mM^{-1} cm^{-2}, which was much more sensitive than the values of previously reported, being 39.89 μA mM^{-1} cm^{-2} [32], 80.4 μA mM^{-1} cm^{-2} [45] and 96.1 μA mM^{-1} cm^{-2} [46]. However, for PDDA-rGO/Pt NDs-modified GC electrode (Fig. 7B), the H_2O_2 concentration was proportional to current response in the range from 0.01 mM to 0.1 mM, the sensitivity reached to 99.2 μA mM^{-1} cm^{-2} and for PDDA-rGO/Pd NPs-modified GC electrode (Fig. 7C), the H_2O_2 concentration was proportional to current response in the range from 0.005 mM to 0.1 mM, the sensitivity reached to 784.6 μA mM^{-1} cm^{-2}. This indicates that bimentallic nannoparticle modified electrode has better performance than monomentallic modified electrode because of the synergic effect of Pt NDs and Pd NPs.

Furthermore, at the signal-to-noise ratio of 3, the detection limit was calculated by 3 × blank variance/slope, 0.027 μM, which was much lower than reported of Se/Pt-modified electrode (3.1 μM) [32], Pt/PPy-modified GC electrode (1.2 μM) [43], Pt/Au/G-CNTs-modified electrode (0.6 μM) [42] and graphene-Pt nanocomposites-modified electrode (0.2 μM) [45]. We have summarized various H_2O_2 sensors in Table 1 which listed the detection limit, the applied potential, and the sensitivity. It is clear that the proposed PDDA-rGO/Pd core-Pt NDs-modified GC electrode exhibits a better performance than many other H_2O_2 sensors.

Chronoamperometry can also be applied to estimate the catalytic rate constant (k_{cat}) for the reaction between PDDA-rGO/Pd core-Pt NDs-modified GC electrode and H_2O_2 according to the equation of Galus [50]:

$$I_C/I_L = \gamma^{1/2}\left[\pi^{1/2}\mathrm{erf}\left(\gamma^{1/2}\right) + \exp\left(-\gamma\right)/\gamma^{1/2}\right] \quad (7)$$

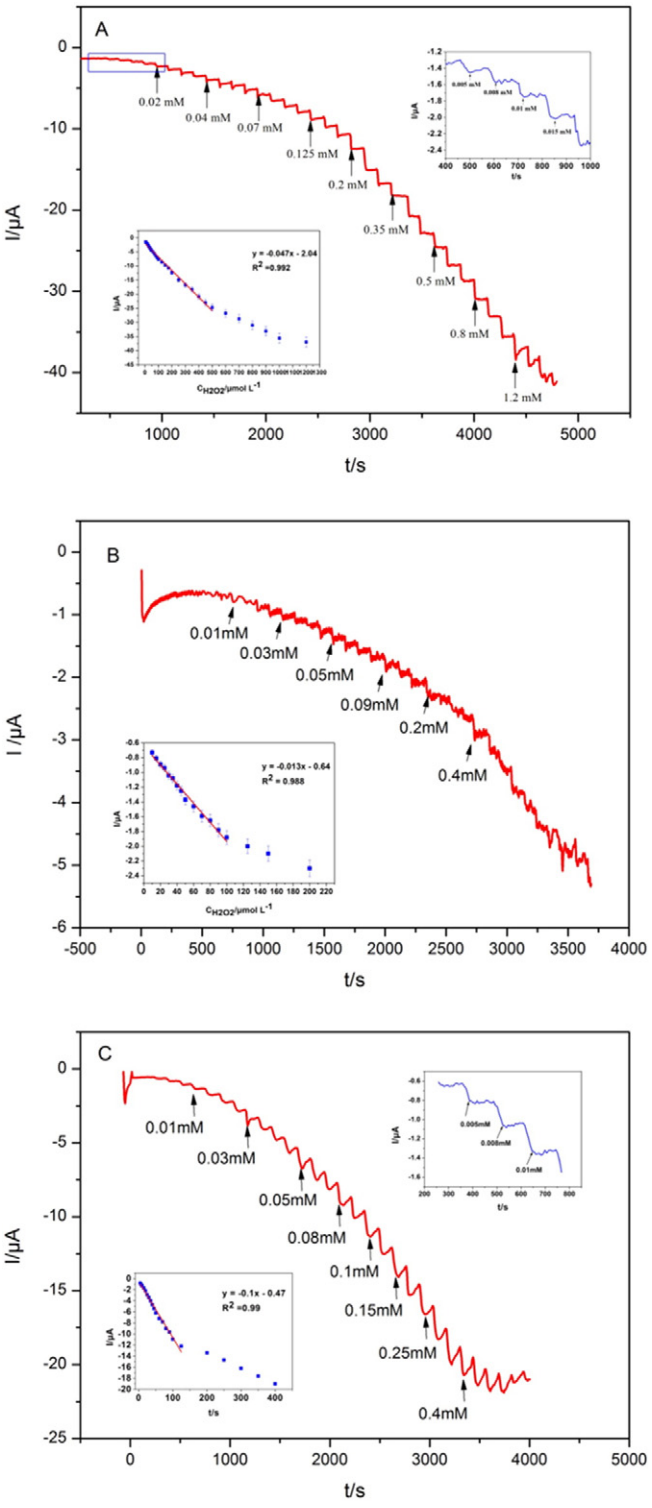

Fig. 7. Amperometric responses of the PDDA-rGO/Pd core-Pt NDs-modified GC electrode (A), PDDA-rGO/Pt NDs-modified GC electrode (B) and PDDA-rGO/Pd NPs-modified GC electrode upon successive addition of H_2O_2 into 0.1 M PBS (pH 7.0) under stirring (applied potential: 18 mV). Error bars = ± standard deviation (n = 5).

where I_C is the catalytic current of H_2O_2, I_L is the limited current in the absence of H_2O_2 and $\gamma = k_{cat}\, C_b\, t$ is the argument of the error function. In cases where γ exceeds the value of 2, the error function is almost equal to 1 and therefore, the above equation can be reduced to:

$$I_C/I_L = \pi^{1/2}\gamma^{1/2} = \pi^{1/2}(k_{cat}\ C_b t)^{1/2} \quad (8)$$

Table 1
Comparison of Pt-based electrodes response to hydrogen peroxide.

Electrode material	Applied potential (V)	Detection limit (μM)	Sensitivity (μA mM^{-1} cm^{-2})	Reference
Se-Pt	**0**	**3.1**	**39.89**	[33]
Pt-PPy[a]	**-**	**1.2**	**80.4**	[45]
Pt NP-PAni[b] hydrogel	**0.56**	**0.7**	**96.1**	[46]
PVA-MWCNTs-Pt NPs	**0**	**0.7**	**122.63**	[48]
Pt-SnO2@C	**0.5**	**0.1**	**241.1**	[49]
Pt-Au-G-CNTs	**0.47**	**0.6**	**313.3**	[44]
GR[c]-Pt	**−0.08**	**0.2**	**459**	[47]
Pd core-Pt NDs-rGO	**0.018**	**0.027**	**672.753**	**This work**

[a] Polypyrrole [b] Polyaniline [c] Graphene.

where t is the time elapsed.

k_{cat} of the catalytic process can be calculated from the slope of I_C/I_L vs. $t^{1/2}$ at a given H_2O_2 concentration. From the values of the slopes, the average value of k_{cat} was estimated to be 1.68×10^5 M^{-1} s^{-1}. Due to high catalytic rate constant, the PDDA-rGO/Pd core-Pt NDs can be used as electron transfer mediator for electrocatalytic reduction of H_2O_2. This shows the superior performance of PDDA-rGO/Pd core-Pt NDs in H_2O_2 detection. Besides, the method of fabricating sensors provides a potential platform for real sample detection in future.

In order to illustrate the practical usage of this sensor, it was applied to detect H_2O_2 in disinfected fetal bovine serum (FBS). The recovery tests for H_2O_2 were performed through addition the standard H_2O_2 of different known concentrations into the FBS samples (Table 2). The recovery was in the range of 95–110% and the relative standard deviation (RSD) ranged from 3.23% to 4.24%, indicating that the sensor could be successfully used for H_2O_2 determination in real sample.

3.5. Selectivity, stability, and reproducibility of the modified electrode

For superior sensors, selectivity is of particular importance. Herein, by comparing the amperometric responses to 0.1 mM ascorbic acid (AA), 0.1 mM cysteine (Cys), 0.1 mM dopamine (DP), 0.1 mM acetaminophen (AP) and 0.1 mM glucose (Glu), the two property of H_2O_2 sensor were studied. As shown in Fig. 8, the current responses to 0.1 mM Cys and 0.1 mM Glu were 0.20 and 0.18 μA, respectively, and the current response to DP, AA and AP could be negligible. Thus, the interference from these compounds could be negligible. Besides, the modified electrode showed acceptable long-term stability and reproducibility.

The reproducibility was evaluated by detecting 5 mM H_2O_2 at five electrodes independently, according to calculate, the relative standard deviation was 3.4%. As showed in Fig. 9, after two weeks, 93% of its original response for H_2O_2 was remained. Therefore, an acceptable long-term stability was exhibited for Pd core-Pt NDs/PDDA-rGO-modified GC electrode.

Table 2
Determination of H_2O_2 in disinfected FBS samples based on PDDA-rGO/Pd core-Pt NDs-modified electrode.

Sample[a]	Added (mM)	Found (mM)	R.S.D. (%, n = 6)	Recovery (%)
1	0.2	0.22	3.23	110
2	0.4	0.41	3.71	102.5
3	0.5	0.48	4.01	96
4	0.8	0.76	3.83	95
5	1.2	1.21	3.67	100.8
6	1.5	1.53	4.24	102

[a] The samples were diluted 100 times with 0.1 M PBS (pH = 7.0).

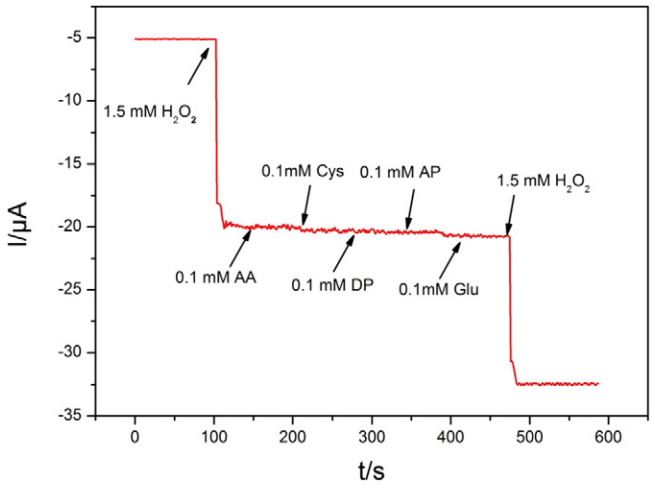

Fig. 8. Amperometric response of PDDA-rGO/Pd core-Pt NDs-modified GC electrode upon successive addition of 1.5 mM H_2O_2, 0.1 mM AA, 0.1 mM Cys, 0.1 mM DP, 0.1 mM AP, 0.1 mM Glu and 1.5 mM H_2O_2. The electrode potential was set at 18 mV versus Ag/AgCl.

4. Conclusions

We synthesized Pd core-Pt NDs nanocomposites by a facile wet-chemical method. A novel non-enzyme sensor was fabricated based on the Pd core-Pt NDs/PDDA-rGO-modified GC electrode, which exhibited much lower detection limit, superior sensitivity and rapid response time in H_2O_2 detection. The excellent selectivity, high electrocatalytic activity and long-term stability of the Pd core-Pt NDs/PDDA-rGO would provide a favorable platform for constructing attractive amperometric sensors and biosensors.

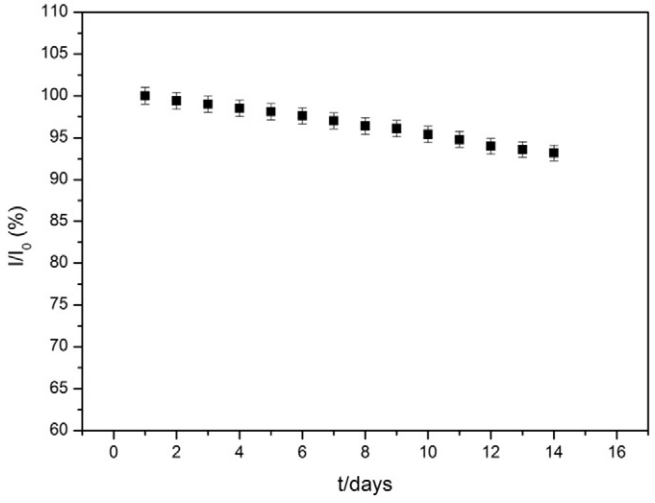

Fig. 9. The stability of PDDA-rGO/Pd core-Pt NDs-modified GC electrode for H_2O_2 on successive 15 days (stored at 4 °C).

Acknowledgments

The financial support from National Natural Science Foundation of China (Grant Nos. 81127001 and 81273993) are acknowledged.

References

[1] A.A. Karyakin, E.E. Karyakina, L. Gorton, Anal. Chem. 72 (2000) 1720–1723.
[2] J. Wang, Y. Lin, L. Chen, Analyst 118 (1993) 277–280.
[3] C. Matsubara, N. Kawamoto, K. Takamura, Analyst 117 (1992) 1781–1784.
[4] L. Luo, Z. Zhang, Anal. Chim. Acta 580 (2006) 14–17.
[5] Z. Rosenzweig, R. Kopelman, Anal. Chem. 68 (1996) 1408–1413.
[6] M.G. Garguilo, N. Huynh, A. Proctor, A.C. Michael, Anal. Chem. 65 (1993) 523–528.
[7] T. Hoshi, H. Saiki, S. Kuwazawa, Y. Kobayashi, J. Anzai, Anal. Sci. 16 (2000) 1009–1010.
[8] A. Safavi, N. Maleki, E. Farjami, Electroanalysis 21 (2009) 1533–1538.
[9] C.M. Welch, C.E. Banks, A.O. Simm, R.G. Compton, Anal. Bioanal. Chem. 382 (2005) 12–21.
[10] Y. Song, K. Cui, L. Wang, S.H. Chen, Nanotechnology 20 (2009) 105501–105508.
[11] L.Y. Cao, Y.L. Liu, B.H. Zhang, L.H. Lu, ACS Appl. Mater. Interfaces 2 (2010) 2339–2346.
[12] P.D. Cozzoli, T. Pellegrino, L. Manna, Chem. Soc. Rev. 35 (2006) 1195–1208.
[13] Y. Kang, X. Ye, J. Chen, Y. Cai, R.E. Diaz, R.R. Adzic, E.A. Stach, C.B. Murray, J. Am. Chem. Soc. 135 (2013) 42–45.
[14] I.J. Plante, S.E. Habas, B.D. Yuhas, D.J. Gargas, T. Mokari, Chem. Mater. 21 (2009) 3662–3667.
[15] S. Stankovich, D.A. Dikin, G.H.B. Dommett, K.M. Kohlhaas, E.J. Zimney, E.A. Stach, R.D. Piner, S.T. Nguyen, R.S. Ruoff, Nature 442 (2006) 282–286.
[16] B.C.H. Steele, A. Heinzel, Materials for fuel-cell technologies, Nature 414 (2001) 345–352.
[17] P. Karam, L.I. Halaoui, Anal. Chem. 80 (2008) 5441–5448.
[18] S. Diezi, D. Ferri, A. Vargas, T. Mallat, A. Baiker, J. Am. Chem. Soc. 128 (2006) 4048–4057.
[19] C. Wang, H. Daimon, Y. Lee, J. Kim, S. Sun, J. Am. Chem. Soc. 129 (2007) 6974–6975.
[20] Z. Chen, M. Waje, W. Li, Y. Yan, Angew. Chem. Int. Ed. 46 (2007) 4060–4063.
[21] E.P. Lee, Z. Peng, D.M. Cate, H. Yang, C.T. Campbell, Y. Xia, J. Am. Chem. Soc. 129 (2007) 10634–10635.
[22] Y. Yamauchi, A. Takai, T. Nagaura, S. Inou, K. Kuroda, J. Am. Chem. Soc. 130 (2008) 5426–5427.
[23] K. Jasuja, V. Berry, ACS Nano 3 (2009) 2358–2366.
[24] J. Liu, L. Cheng, Y. Song, B. Liu, S. Dong, Langmuir 17 (2001) 6747–6750.
[25] M. Pumera, Chem. Soc. Rev. 39 (2010) 4146–4157.
[26] J. Zhu, M. Chen, Q. He, L. Shao, S. Wei, Z. Guo, RSC Adv. 3 (2013) 22790–22824.
[27] Y. Wang, Y.M. Li, L.H. Tang, J. Lu, J.H. Li, Electrochem. Commun. 11 (2009) 889–892.
[28] M. Zhou, Y.M. Zhai, S.J. Dong, Anal. Chem. 81 (2009) 5603–5613.
[29] D. Zhang, Y.X. Fang, Z. Miao, M. Ma, X. Du, S. Takahashi, J. Anzai, Q. Chen, Electrochim. Acta 107 (2013) 656–663.
[30] T. Aizawa, R. Souda, S. Otani, Y. Ishizawa, C. Oshima, Phys. Rev. Lett. 64 (1990) 768–771.
[31] K.S. Novoselov, A.K. Geim, S.V. Morozov, D. Jiang, Y. Zhang, S.V. Dubonos, I.V. Grigorieva, A.A. Firsov, Science 306 (2004) 666–669.
[32] C. Berger, Z. Song, X. Li, X. Wu, N. Brown, C. Naud, D. Mayou, T. Li, J. Hass, A.N. Marchenkov, E.H. Conrad, P.N. First, W.A. de Heer, Science 312 (2006) 1191–1196.
[33] S. Park, R.S. Ruoff, Nat. Nanotechnol. 4 (2009) 217–224.
[34] M. Lotya, Y. Hernandez, P.J. King, R.J. Smith, V. Nicolosi, L.S. Karlsson, F.M. Blighe, S. De, Z. Wang, I.T. McGovern, G.S. Duesberg, J.N. Coleman, J. Am. Chem. Soc. 131 (2009) 3611–3620.
[35] B. Lim, M.J. Jiang, P.H.C. Camargo, E.C. Cho, J. Tao, X.M. Lu, Y.M. Zhu, Y.N. Xia, Science 324 (2009) 1302–1305.
[36] L.C. Ciacchi, W. Pompe, J. Phys. Chem. B 107 (2003) 1755–1764.
[37] X. Teng, X. Liang, S. Maksimuk, H. Yang, Small 2 (2006) 249–253.
[38] E. Matijevic, Chem. Mater. 5 (1993) 412–426.
[39] Y. Li, R. Yuan, Y.Q. Chai, Z.J. Song, Electrochim. Acta 56 (2011) 6715–6721.
[40] X. Gao, W. Wei, L. Yang, M. Guo, Electroanalysis 18 (2006) 485–492.
[41] Y. Mukouyama, S. Nakanishi, H. Konishi, K. Karasumi, Y. Nakato, Phys. Chem. Chem. Phys. 3 (2001) 3284–3289.
[42] E. Lavion, J. Electroanal. Chem. 101 (1979) 19.
[43] J.A. Harrison, Z.A. Khan, J. Electroanal. Chem. 28 (1970) 131–138.
[44] D.B. Lu, Y. Zhang, S.X. Lin, L.T. Wang, C.M. Wang, Talanta 112 (2013) 111–116.
[45] X. Bian, X. Lu, E. Jin, L. Kong, W. Zhang, C. Wang, Talanta 81 (2010) 813–818.
[46] D. Zhai, B. Liu, Y. Shi, L. Pan, Y. Wang, W. Li, R. Zhang, G. Yu, ACS Nano 7 (2013) 3540–3546.
[47] Y. Zhang, X. Bai, X. Wang, K.K. Shiu, Y. Zhu, H. Jiang, Anal. Chem. 86 (2014) 9459–9465.
[48] Y.X. Fang, D. Zhang, X. Qin, Z.Y. Miao, S. Takahashi, J. Anzai, Q. Chen, Electrochim. Acta 70 (2012) 266–271.
[49] H.T. Lu, S. Yu, Y. Fan, C.P. Yang, D.L. Xu, Colloids Surf. B Biointerfaces 101 (2013) 106–110.
[50] Z. Galus, Fundamentals of Electrochemical Analysis, Ellis Horwood, New York, 1976.